

1

## **Iodine chemistry after dark**

2 Alfonso Saiz-Lopez<sup>1</sup>, John M.C. Plane<sup>2</sup>, Carlos A. Cuevas<sup>1</sup>, Anoop S. Mahajan<sup>3</sup>, Jean-François  
3 Lamarque<sup>4</sup> and Douglas E. Kinnison<sup>4</sup>

4 <sup>1</sup>Department of Atmospheric Chemistry and Climate, Institute of Physical Chemistry  
5 Rocasolano, CSIC, Madrid, Spain

6  
7 <sup>2</sup>School of Chemistry, University of Leeds, Leeds, UK

8  
9 <sup>3</sup>Indian Institute of Tropical Meteorology, Pune, India

10  
11 <sup>4</sup>Atmospheric Chemistry Observations and Modelling, NCAR, Colorado, USA

12 Correspondence to: A. Saiz-Lopez (a.saiz@csic.es)

1 **Abstract**

2 Little attention has so far been paid to the nighttime atmospheric chemistry of iodine species.  
3 Current atmospheric models predict a buildup of HOI and I<sub>2</sub> during the night that leads to a spike  
4 of IO at sunrise, which is not observed by measurements. In this work, electronic structure  
5 calculations are used to survey possible reactions that HOI and I<sub>2</sub> could undergo at night in the  
6 lower troposphere, and hence reduce their nighttime accumulation. The new reaction NO<sub>3</sub> + HOI  
7 → IO + HNO<sub>3</sub> is proposed, with a rate coefficient calculated from statistical rate theory over the  
8 temperature range 260 - 300 K and at a pressure of 1000 hPa to be  $k(T) = 2.7 \times 10^{-12} (300 \text{ K} / T$   
9  $)^{2.66} \text{ cm}^3 \text{ molecule}^{-1} \text{ s}^{-1}$ . This reaction is included in two atmospheric models, along with the  
10 known reaction between I<sub>2</sub> and NO<sub>3</sub>, to explore a new nocturnal iodine radical activation  
11 mechanism. The results show that this iodine scheme leads to a considerable reduction of  
12 nighttime HOI and I<sub>2</sub>, which results in the enhancement of more than 25% of nighttime ocean  
13 emissions of HOI + I<sub>2</sub> and the removal of the anomalous spike of IO at sunrise. We suggest that  
14 active nighttime iodine can also have a considerable, so far unrecognized, impact on the  
15 reduction of the NO<sub>3</sub> radical levels in the marine boundary layer (MBL) and hence upon the  
16 nocturnal oxidizing capacity of the marine atmosphere. The effect of this is exemplified by the  
17 indirect effect on dimethyl sulfide (DMS) oxidation.

18

19

20

21

## 1 **1. Introduction**

2 Active nighttime iodine chemistry was first evidenced a decade ago when it was shown that  
3 nocturnal  $I_2$  emitted by macroalgae could react with  $NO_3$  leading to the formation of IO and  
4 OIO, which were measured in the coastal MBL at Mace Head, Ireland (Saiz-Lopez and Plane,  
5 2004). The nitrate radical has also been recently suggested as a nocturnal loss of  $CH_2I_2$ , which  
6 helps to reconcile observed and modelled concentrations of this iodocarbon over the remote  
7 MBL (Carpenter et al., 2015). However, most of the work on reactive atmospheric iodine has  
8 focused on the use of daytime observations and models to assess its role in the catalytic  
9 destruction of ozone and the oxidizing capacity of the troposphere (e.g. Saiz-Lopez et al. (2012b)  
10 and references therein). In the MBL, iodine-, along with bromine-catalysed ozone destruction  
11 contributes up to 45% of the observed daytime depletion (Mahajan et al., 2010a; Read et al.,  
12 2008), although this contribution shows large geographical variability (Gómez Martín et al.,  
13 2013; Mahajan et al., 2012; Prados-Roman et al., 2015b; Volkamer et al., 2015). Iodine  
14 compounds have also been implicated in the formation of aerosols, although the mechanisms and  
15 magnitudes of these processes are not fully understood (Allan et al., 2015; Gomez Martin et al.,  
16 2013; Hoffmann et al., 2001; McFiggans et al., 2004; O'Dowd et al., 2002; Roscoe et al., 2015).  
17 Reactive forms of inorganic iodine may also contribute to the oxidation of elemental mercury  
18 over the tropical oceans (Wang et al., 2014). In recent years, iodine sources and chemistry have  
19 also been implemented in global models demonstrating the effect of iodine chemistry in the  
20 oxidation capacity of the global marine troposphere (Ordóñez et al., 2012; Saiz-Lopez et al.,  
21 2012a; Saiz-Lopez et al., 2014; Sherwen et al., 2016).

22 Iodine is emitted into the atmosphere from the ocean surface in both organic and inorganic  
23 forms. The main organic compounds emitted are methyl iodide ( $CH_3I$ ), ethyl iodide ( $C_2H_5I$ ),

1 propyl iodide (1- and 2-C<sub>3</sub>H<sub>7</sub>I), chloriodomethane (CH<sub>2</sub>ICl), bromiodomethane (CH<sub>2</sub>IBr), and  
2 diiodomethane (CH<sub>2</sub>I<sub>2</sub>) (Butler et al., 2007; Carpenter, 2003; Jones et al., 2010; Mahajan et al.,  
3 2012). However, these organic compounds contribute only up to a fourth of the MBL iodine  
4 loading (Großmann et al., 2013; Jones et al., 2010; Mahajan et al., 2010a; Prados-Roman et al.,  
5 2015b). Inorganic emissions of HOI and I<sub>2</sub>, which result from the deposition of O<sub>3</sub> at the ocean  
6 surface and subsequent reaction with I<sup>-</sup> ions in the surface microlayer, account for the main  
7 source of iodine in the MBL (Carpenter et al., 2013). Recent laboratory experiments have shown  
8 that HOI is the major compound emitted, and provided parameterizations of the fluxes of both  
9 species depending on wind speed, temperature, and the concentrations of O<sub>3</sub> and I<sup>-</sup> (Carpenter et  
10 al., 2013; MacDonald et al., 2014). These parameterized fluxes of HOI and I<sub>2</sub> have then been  
11 used in a one-dimensional model to study the diurnal evolution of the IO and I<sub>2</sub> mixing ratios at  
12 the Cape Verde Atmospheric Observatory (CVAO) (Carpenter et al., 2013; Lawler et al., 2014).  
13 The model simulations replicate well the levels and general diurnal profiles of IO and I<sub>2</sub>,  
14 although an early morning ‘dawn spike’ in IO is predicted by the models, but has not been  
15 observed (Mahajan et al., 2010a; Read et al., 2008). The morning peak predicted by current  
16 iodine chemistry models is due to a buildup of the emitted I<sub>2</sub> and HOI (which is converted into  
17 I<sub>2</sub>/IBr/ICl through heterogeneous sea-salt recycling) over the course of the night, followed by  
18 rapid photolysis at sunrise.

19 Traditionally it has been thought that iodine chemistry has a negligible effect on oxidizing  
20 capacity of the nocturnal marine atmosphere. As a consequence, unlike the demonstrated effect  
21 of iodine on the levels of daytime oxidants, the impact of active iodine upon the main nighttime  
22 oxidant, NO<sub>3</sub>, remains an open question. This is important given that in many parts of the ocean  
23 the NO<sub>3</sub> + DMS reaction is at least as important as OH + DMS in oxidizing DMS (Allan et al.,

1 2000), and hence a reduction of NO<sub>3</sub> may have an effect in the production of SO<sub>2</sub> and methane  
2 sulfonic acid (MSA). Here, we discuss possible mechanisms of nighttime iodine radical  
3 activation and their potential effect on nighttime iodine ocean fluxes and the currently modeled  
4 dawn spike in IO. A new reaction of HOI with NO<sub>3</sub> is proposed, supported by theoretical  
5 calculations. We explore the implications of this new reaction both for iodine and NO<sub>3</sub>  
6 chemistries.

7

## 8 **2. Nocturnal iodine radical activation mechanism**

9 We use the reaction mechanism that has recently been described in a global modelling study by  
10 Saiz-Lopez et al. (2014) (see supplementary information). In addition to the reactions included in  
11 that scheme, we also include nighttime gas-phase reactions based on the theoretical calculations  
12 described below. The additional reactions are listed in Table 1 and a scheme with this new  
13 nocturnal chemistry is included in Figure 1.

14 To the best of our knowledge, reactions of HOI specific to night time have not been studied,  
15 either theoretically or through laboratory experiments. Currently, HOI is thought to build up  
16 overnight until sunrise, with only heterogeneous uptake on seasalt aerosol as a nighttime loss  
17 process (Saiz-Lopez et al., 2012b; Simpson et al., 2015). In addition to the well known I<sub>2</sub> + NO<sub>3</sub>  
18 reaction (R1) (Chambers et al., 1992), here we consider several possible HOI reactions that could  
19 occur at night, in the absence of photolysis and OH:





1 The stationary points on the potential energy surface (PES) for reaction 4 are illustrated in Figure  
2 3. HOI and NO<sub>3</sub> associate to form a complex which is 24 kJ mol<sup>-1</sup> below the reactant entrance  
3 channel. H-atom transfer involves a submerged transition state to form a IO--HNO<sub>3</sub> complex,  
4 which can then dissociate to the products IO + HNO<sub>3</sub>. Overall, the reaction is exothermic by 11  
5 kJ mol<sup>-1</sup>. The vibrational frequencies, rotational energies and geometries (in Cartesian  
6 co-ordinates) of these intermediates are listed in Table 2.

7 The rate coefficient for reaction 4 was then estimated using Rice-Ramsperger-Kassel-Markus  
8 (RRKM) theory, employing a multi-well energy-grained master equation solver based on the  
9 inverse Laplace transform method - MESMER (Master Equation Solver for Multi-well Energy  
10 Reactions) (Roberston et al., 2014). The reaction proceeds via the formation of the excited  
11 HOI--NO<sub>3</sub> complex from HOI + NO<sub>3</sub>. This complex can then dissociate back to the reactants or  
12 rearrange to the IO--HNO<sub>3</sub> intermediate complex over the transition state, which can in turn  
13 dissociate to the products IO + HNO<sub>3</sub>. Either of the intermediates can also be stabilized by  
14 collision with the third body (N<sub>2</sub>). The time evolution of all these possible outcomes is modelled  
15 using the master equation.

16 The internal energies of the intermediates on the PES were divided into a contiguous set of  
17 grains (width 10 cm<sup>-1</sup>), each containing a bundle of rovibrational states calculated with the  
18 molecular parameters in Table 2. It should be noted that the HOI-NO<sub>3</sub> and IO-HNO<sub>3</sub> complexes  
19 both have low frequency vibrational modes (< 100 cm<sup>-1</sup>) which should more correctly be treated  
20 as hindered rotors rather than vibrations. However, in our experience this is not worth doing this  
21 until experimental rate coefficients are available to fit the rotor barrier heights. In any case, the  
22 energies of both complexes are far enough below the energy of the entrance channel (figure 3)  
23 that relatively small changes in their densities of states will have a minor effect on the overall

1 rate coefficient. Each grain was then assigned a set of microcanonical rate coefficients linking it  
2 to other intermediates, calculated by RRKM theory. For dissociation to products or reactants,  
3 microcanonical rate coefficients were determined using inverse Laplace transformation to link  
4 them directly to the capture rate coefficient,  $k_{\text{capture}}$ . For reaction 4 and the reverse reaction IO +  
5 HNO<sub>3</sub> involving neutral species,  $k_{\text{capture}}$  was set to a typical capture rate coefficient of  $2.5 \times 10^{-10}$   
6  $(T/300 \text{ K})^{1/6} \text{ cm}^3 \text{ molecule}^{-1} \text{ s}^{-1}$ , where the small positive temperature dependence is  
7 characteristic of a long-range potential governed by dispersion and dipole-dipole forces  
8 (Georgievskii and Klippenstein, 2005).

9 The probability of collisional transfer between grains was estimated using the exponential down  
10 model, where the average energy for downward transitions was set to  $\langle \Delta E \rangle_{\text{down}} = 300 \text{ cm}^{-1}$  for  
11 N<sub>2</sub> as the third body (Gilbert and Smith, 1990). MESMER determines the temperature- and  
12 pressure-dependent rate coefficient from the full microcanonical description of the system time  
13 evolution by performing an eigenvector/eigenvalue analysis (Bartis and Widom, 1974). The  
14 resulting rate coefficient over the temperature range 260 - 300 K at a pressure of 1000 hPa is  
15  $k_4(T) = 2.7 \times 10^{-12} (300 \text{ K} / T)^{2.66} \text{ cm}^3 \text{ molecule}^{-1} \text{ s}^{-1}$ . Because the intermediate complexes are  
16 not strongly bound, and the transition state and products are below the entrance channel, the only  
17 products formed in reaction 4 under atmospheric conditions are IO + HNO<sub>3</sub>. The absence of a  
18 barrier above the entrance channel, and the fact that the intermediate complexes and barrier are  
19 well below the entrance channel within their uncertainties, means that the uncertainty in  $k_4$   
20 principally arises from the estimated capture rate coefficient and so is likely to be no more than a  
21 factor of 2.

22 Note that NO<sub>3</sub> also reacts with CH<sub>2</sub>I<sub>2</sub> with a rate constant  $\sim 2\text{-}4 \times 10^{-13} \text{ cm}^3 \text{ molecule}^{-1} \text{ s}^{-1}$ , which  
23 can have a significant effect on nighttime CH<sub>2</sub>I<sub>2</sub> concentration (Carpenter et al., 2015). However



1 the products of this reaction are still uncertain (Carpenter et al., 2015; Nakano et al., 2006) and  
2 its rate is considerably slower than that of R4.

3 In summary, the only likely gas-phase reactions that I<sub>2</sub> and HOI undergo in the nighttime  
4 troposphere are R1 and R4, respectively. These are included in the model reaction scheme to  
5 examine their impacts on the evolution of iodine species in the atmosphere.

6

#### 7 **4. Atmospheric modelling**

8 We use two atmospheric chemical transport models to study *i*) the impact of this new chemistry  
9 on the nighttime chemistry and partitioning of iodine species, and *ii*) the resulting geographical  
10 distribution of nocturnal iodine and impact on NO<sub>3</sub> within the global marine boundary layer.

11 The first model, Tropospheric HALogen chemistry MOdel (THAMO), is used for a detailed  
12 kinetics study of the impact of the different reactions shown in Table 1 as well as to assess which  
13 uptake rates best reproduce observations from a field study at the CVAO (Carpenter et al., 2011).

14 THAMO has been used in the past to study iodine chemistry at the CVAO and further details  
15 including the full chemical scheme can be found elsewhere (Lawler et al., 2014; Mahajan et al.,  
16 2009; Mahajan et al., 2010a; Mahajan et al., 2010b; Read et al., 2008; Saiz-Lopez et al., 2008).

17 Briefly, THAMO is a 1-D chemistry transport model with 200 stacked boxes at a vertical  
18 resolution of 5m (total height 1 km). The model treats iodine, bromine, O<sub>3</sub>, NO<sub>x</sub> and HO<sub>x</sub>

19 chemistry, and is constrained with typical measured values of other chemical species in the  
20 MBL: [CO]=110 nmol mol<sup>-1</sup>; [DMS]=30 pmol/mol; [CH<sub>4</sub>]=1820 nmol mol<sup>-1</sup>; [ethane]=925  
21 pmol/mol; [CH<sub>3</sub>CHO]=970 pmol/mol; [HCHO]=500 pmol/mol; [isoprene]=10 pmol/mol;

22 [propane]=60 pmol/mol; [propene]=20 pmol/mol. The average background aerosol surface area

1 (ASA) used is  $1 \times 10^{-6} \text{ cm}^2 \text{ cm}^{-3}$  (Lee et al., 2009; Lee et al., 2010; Read et al., 2008; Read et al.,  
2 2009). The model is initialized at midnight and the evolution of iodine species,  $\text{O}_3$ ,  $\text{NO}_x$  and  $\text{HO}_x$   
3 is followed until the model reaches steady state.

4 The second model is the global 3D chemistry-climate model CAM-Chem (Community  
5 Atmospheric Model with chemistry, version 4.0), which is used to study the impact of reactions  
6 1 and 4 on a global scale. The model includes a comprehensive chemistry scheme to simulate the  
7 evolution of trace gases and aerosols in the troposphere and the stratosphere (Lamarque et al.,  
8 2012). The model runs with the iodine and bromine chemistry schemes from previous studies  
9 (Fernandez et al., 2014; Saiz-Lopez et al., 2014; Saiz-Lopez et al., 2015), including the  
10 photochemical breakdown of bromo- and iodo-carbons emitted from the oceans (Ordóñez et al.,  
11 2012) and abiotic oceanic sources of HOI and  $\text{I}_2$  (Prados-Roman et al., 2015a). CAM-Chem has  
12 been configured in this work with a horizontal resolution of  $1.9^\circ$  latitude by  $2.5^\circ$  longitude and 26  
13 vertical levels, from the surface to  $\sim 40\text{km}$  altitude. All model runs in this study were performed  
14 in the specified dynamics mode (Lamarque et al., 2012) using offline meteorological fields  
15 instead of an online calculation, to allow direct comparisons between different simulations. This  
16 offline meteorology consists of a high frequency meteorological input from a previous free  
17 running climatic simulation.

18 It should be noted that during nighttime the uptake on aerosols of emitted species such as  $\text{I}_2$  and  
19 HOI, and the uptake of reservoir species such as  $\text{IONO}_2$ , can play a major role in the cycling of  
20 iodine. Observations at CVAO show that  $\text{I}_2$  peaked at about 1 pmol/mol during the night and that  
21 ICl was not detected above the 1 pmol/mol detection limit of the instrument (Lawler et al.,  
22 2014). In order to match these observations, we need to reduce the uptake and heterogeneous  
23 recycling of iodine species. The uptake rates of chemical species on the background seasalt

1 aerosols are determined by their uptake coefficients ( $\gamma$ ). The database of mass accommodation  
2 and/or uptake coefficients is rather sparse and essentially limited to  $I_2$ , HI, HOI, ICl, IBr on pure  
3 water/ice and on sulphuric acid particles (Sander et al., 2006). Other iodine species which are  
4 likely to undergo uptake onto aerosol are OIO, HIO<sub>3</sub>, INO<sub>2</sub>, IONO<sub>2</sub>, I<sub>2</sub>O<sub>2</sub> (Saiz-Lopez et al.,  
5 2012a; Sommariva et al., 2012). Uptake of HOI is very uncertain, with  $\gamma(\text{HOI})$  ranging from  $2 \times$   
6  $10^{-3}$  to 0.3 depending on the surface composition and state (Holmes et al., 2001). Sommariva et  
7 al. (2012) assumed  $\gamma(\text{HOI})$  to be 0.6, similar to the value for HOBr measured by Wachsmuth et  
8 al. (2002). In the case of IONO<sub>2</sub>, the uptake coefficient has not been measured, with most models  
9 using values of 0.1 (Lawler et al., 2014; Leigh et al., 2010; Mahajan et al., 2009; Mahajan et al.,  
10 2010a; Mahajan et al., 2010b; Saiz-Lopez et al., 2008; Sommariva et al., 2012; von Glasow et  
11 al., 2002). The modelled levels of  $I_2$  and ICl change with different values of uptake coefficients.  
12 To match the CVAO  $I_2$  and ICl observations (Lawler et al., 2014), we have used  $\gamma = 0.01$  for  
13 HOI and IONO<sub>2</sub>, which is within the uncertainty in the literature, and assumed that 80% is  
14 recycled as  $I_2$ . Further measurements of these dihalogen species are needed to better constrain  
15 their heterogeneous recycling on seasalt aerosols.

16

## 17 **5. Results and discussion**

18 Of the possible nocturnal iodine activation reactions involving the inorganic iodine source gases  
19  $I_2$  and HOI, only reactions R1 and R4 appear to be likely candidates (see Section 3). We  
20 therefore designed two modelling scenarios: Scenario 1 (S1), without nighttime reactions of  $I_2$  or  
21 HOI with NO<sub>3</sub>; and Scenario 2 (S2), including reactions R1 and R4 for the degradation of HOI  
22 and  $I_2$  by NO<sub>3</sub>. In the one-dimensional model THAMO, the  $I_2$  and HOI are injected into the

1 atmosphere from the ocean surface using the flux parameterizations derived from laboratory  
2 experiments (Carpenter et al., 2013; MacDonald et al., 2014). Figure 4 shows the resulting  
3 diurnal evolution of the HOI and I<sub>2</sub> mixing ratios in the two scenarios. The I<sub>2</sub> mixing ratio peaks  
4 during the night in both the scenarios due to quick loss by photolysis during the daytime. By  
5 contrast, HOI is present during daytime due to its production through the reaction of IO with  
6 HO<sub>2</sub>, and peaks just before sunset. In the first scenario, without the inclusion of reactions R1 and  
7 R4, Figure 4 (right-hand side panels) shows that HOI and I<sub>2</sub> both build up during the night,  
8 reaching a concentration peak just before dawn. This is especially noticeable for I<sub>2</sub> as the  
9 daytime concentrations are much lower than during the night. For both species, inclusion of  
10 reactions with NO<sub>3</sub> causes a decrease in their respective nocturnal concentrations (Fig. 4, left-  
11 hand side panels). The inclusion of reactions R1 and R4 also leads to a modelled I<sub>2</sub> concentration  
12 which is in better agreement with the observations of the molecule made at CVAO (Lawler et  
13 al., 2014), reaching peak values of about 1 pmol/mol, as compared to about 3 pmol/mol for the  
14 scenario without nighttime reactions. An additional consequence of including reactions R1 and  
15 R4 is the significant increase of the sea-air fluxes of HOI and I<sub>2</sub> at night due to their atmospheric  
16 removal by NO<sub>3</sub> (Fig. 4, bottom panel).

17 Figure 5 shows the diurnal evolution of IO, NO<sub>3</sub> and IONO<sub>2</sub> in both model scenarios. Although  
18 the daytime peak values of IO are well reproduced in both scenarios, reaching about 1.5  
19 pmol/mol around noon similar to the ground-based observations (Read et al., 2008), the inclusion  
20 of reactions R1 and R4 leads to the removal of the dawn spike in IO, which is predicted by  
21 current iodine models but was not observed at CVAO (Mahajan et al., 2010a; Read et al., 2008).  
22 The IO dawn spike predicted by models is due to a buildup of the emitted I<sub>2</sub> and HOI (which is  
23 converted into I<sub>2</sub>/IBr/ICl through heterogeneous recycling) over the night, followed by rapid

1 photolysis after first sunlight. However, due to the considerable removal of HOI and I<sub>2</sub> through  
2 the night due to reaction with ambient NO<sub>3</sub>, this spike does not appear in the second scenario,  
3 leading to a modification of the diurnal profile of IO that better matches with observations.

4 Reactions R1 and R4 also reduce the NO<sub>3</sub> mixing ratio (Fig. 5, middle panels). In scenario 1, the  
5 NO<sub>3</sub> is modelled to peak at about 14 pmol/mol just before dawn. However, the inclusion of  
6 reactions R1 and R4 leads to near complete depletion of NO<sub>3</sub> close to the surface, with the peak  
7 level at the surface reaching only 2 pmol/mol, since reactions R1 and R4 become the main  
8 atmospheric loss processes for NO<sub>3</sub> in the lower MBL. These reactions lead however to the  
9 buildup of IONO<sub>2</sub> during the night (Fig. 5, bottom panels). In the absence of reactions R1 and  
10 R4, significant levels of IONO<sub>2</sub> are seen only at dawn and dusk since no other reactions produce  
11 IONO<sub>2</sub> at night, and during the day IONO<sub>2</sub> is removed by photolysis. However, with continuous  
12 conversion of I<sub>2</sub> and HOI to IONO<sub>2</sub> by reactions R1 and R4 in scenario 2, IONO<sub>2</sub> is modelled to  
13 reach up to 3 pmol/mol in the nocturnal MBL.

14 Given the associated uncertainty in the theoretical estimate of the  $k_4$ , we used THAMO to assess  
15 the sensitivity of surface NO<sub>3</sub> to  $k_4$ . Figure 6 shows that NO<sub>3</sub> is in fact highly coupled to  $k_4$ , with  
16 the expected uncertainty in  $k_4$  of one order of magnitude (see above) giving rise to a factor of two  
17 change in NO<sub>3</sub>. A laboratory measurement of  $k_4$  should therefore be undertaken in the future.

18 We now implement the nighttime reactions in the 3D global model (CAM-Chem) to assess the  
19 resulting geographical distributions and impacts of these reactions. We have also run two  
20 different scenarios in CAM-Chem, the first without R1 and R4 in the chemical scheme, and the  
21 second including the new nighttime iodine chemistry. Figure 7 shows how the inclusion of R1  
22 and R4 reduces globally the nighttime concentrations of I<sub>2</sub> and HOI. The plots correspond to the

1 nighttime averaged (from 00LT to 01LT) differences between the model scenarios. Considerable  
2 reductions of up to 0.5 and 10 pmol/mol (i.e. up to 100% removal) are observed for I<sub>2</sub> and HOI,  
3 respectively, particularly over coastal polluted regions where continental pollution outflow leads  
4 to higher levels of NO<sub>3</sub> in the nighttime MBL. Major shipping routes also show strong nocturnal  
5 iodine activity due to the characteristically high NO<sub>x</sub>, and resulting NO<sub>3</sub>, associated with  
6 shipping emissions.

7 Figure 8 shows the effect of this nocturnal chemistry on the concentrations of IONO<sub>2</sub> and NO<sub>3</sub>.  
8 As in the previous figure, the plots correspond to the nighttime averaged difference between the  
9 second and the first scenarios. The maps show an increase of IONO<sub>2</sub> of up to 15 pmol/mol  
10 (~600%) over polluted coastal areas, due to efficient conversion of NO<sub>3</sub> into IONO<sub>2</sub>. The bottom  
11 panel of Figure 7 shows the expected decrease of NO<sub>3</sub> levels associated with the inclusion of  
12 reactions R1 and R4, with decreases of up to ~4 pmol/mol (up to 60%) over marine polluted  
13 regions. We model global percentage reductions in the NO<sub>3</sub> concentrations of 7.1% (60S-60N),  
14 with nitrate removal of up to 80% in non-polluted remote oceanic regions with low NO<sub>3</sub> levels.  
15 This in turn can affect the modelled oxidation of DMS by NO<sub>3</sub>. We estimate that the reduction in  
16 NO<sub>3</sub>, due to the inclusion of R1 and R4, results in a model increase in DMS levels of up to 7  
17 pmol/mol (about 20%) in marine regions affected by continental pollution outflow (Fig. 9). We  
18 therefore suggest that the inclusion of the new nighttime iodine chemistry can have a large, so far  
19 unrecognized, impact on the nocturnal oxidizing capacity of the marine atmosphere.

20 The hourly evolution of the main species involved in this study is shown in Figures 10 and 11,  
21 which include the levels of HOI, I<sub>2</sub>, IONO<sub>2</sub> and NO<sub>3</sub> in the MBL over regions where nocturnal  
22 iodine is modelled to be particularly active. The first region is located within the Mediterranean  
23 Sea, an area that shows large differences during the summer months when high ozone levels

1 drive large emissions of HOI and I<sub>2</sub> from the sea, and the high levels of NO<sub>3</sub> at nighttime make  
2 this chemistry especially important. The hourly average in August is shown in Figure 10 for  
3 HOI, IONO<sub>2</sub> and I<sub>2</sub>. HOI and IONO<sub>2</sub> (Fig 10 ) are the species whose concentration differ most  
4 between scenarios as HOI is removed and IONO<sub>2</sub> produced by R4 (and, to a lesser extent, R1).  
5 Over a Pacific Ocean region at the south of the Baja California Peninsula, the modelled  
6 differences between the two scenarios are even higher than over the Mediterranean Sea (Figure  
7 11). Large differences in MBL NO<sub>3</sub>, up to 28%, are modelled during the night caused by  
8 pollution outflow from the west coasts of Mexico and USA.

9

## 10 **6. Summary and conclusions**

11 The viability of the reaction of HOI with NO<sub>2</sub>, HNO<sub>3</sub> and NO<sub>3</sub> has been studied by theoretical  
12 calculations. The results indicate that only the reaction of HOI with NO<sub>3</sub>, to yield IO + HNO<sub>3</sub>, is  
13 possible under tropospheric conditions. The inclusion of this reaction, along with that of I<sub>2</sub> +  
14 NO<sub>3</sub>, has a number of significant implications: *i*) nocturnal iodine radical chemistry is activated;  
15 *ii*) this causes enhanced nighttime oceanic emissions of HOI and I<sub>2</sub>; *iii*) nighttime iodine species  
16 are partitioned into high levels of IONO<sub>2</sub>; *iv*) the IO spike, modelled by current iodine models  
17 but not shown by observations, is removed; and, *v*) a reduction of the levels of nitrate radical in  
18 the MBL, with the associated less efficient oxidation of DMS, which has important implications  
19 for our understanding of the nocturnal oxidizing capacity of the marine atmosphere.

20

21

## 1 **Acknowledgments**

2 This work was supported by the Spanish National Research Council (CSIC). The National  
3 Center for Atmospheric Research (NCAR) is funded by the National Science Foundation NSF.  
4 The Climate Simulation Laboratory at NCAR's Computational and Information Systems  
5 Laboratory (CISL) provided the computing resources (ark:/85065/d7wd3xhc). As part of the  
6 CESM project, CAM-Chem is supported by the NSF and the Office of Science (BER) of the US  
7 Department of Energy. This work was also sponsored by the NASA Atmospheric Composition  
8 Modeling and Analysis Program Activities (ACMAP, number NNX11AH90G).

9

## 10 **References**

11 Allan, B. J., McFiggans, G., Plane, J. M. C., Coe, H., and McFadyen, G. G.: The nitrate radical  
12 in the remote marine boundary layer, *Journal of Geophysical Research: Atmospheres*, 105,  
13 24191-24204, 10.1029/2000jd900314, 2000.

14 Allan, J. D., Williams, P. I., Najera, J., Whitehead, J. D., Flynn, M. J., Taylor, J. W., Liu, D.,  
15 Darbyshire, E., Carpenter, L. J., Chance, R., Andrews, S. J., Hackenberg, S. C., and McFiggans,  
16 G.: Iodine observed in new particle formation events in the Arctic atmosphere during  
17 ACCACIA, *Atmos. Chem. Phys.*, 15, 5599-5609, 10.5194/acp-15-5599-2015, 2015.

18 Bartis, J. T., and Widom, B.: Stochastic models of the interconversion of three or more chemical  
19 species, *J. Chem. Phys.*, 60, 3474-3482, doi: 10.1063/1.1681562, 1974.

20 Butler, J. H., King, D. B., Lobert, J. M., Montzka, S. A., Yvon-Lewis, S. A., Hall, B. D.,  
21 Warwick, N. J., Mondeel, D. J., Aydin, M., and Elkins, J. W.: Oceanic distributions and



1 emissions of short-lived halocarbons, *Global Biogeochem. Cycles*, 21, GB1023,  
2 10.1029/2006gb002732, 2007.

3 Carpenter, L. J.: Iodine In the marine Boundary Layer, *Chem. Rev.*, 103 (12), 4953-4962, 2003.

4 Carpenter, L. J., Fleming, Z. L., Read, K. A., Lee, J. D., Moller, S. J., Hopkins, J. R., Purvis, R.  
5 M., Lewis, A. C., Müller, K., Heinold, B., Herrmann, H., Fomba, K. W., Pinxteren, D., Müller,  
6 C., Tegen, I., Wiedensohler, A., Müller, T., Niedermeier, N., Achterberg, E. P., Patey, M. D.,  
7 Kozlova, E. A., Heimann, M., Heard, D. E., Plane, J. M. C., Mahajan, A., Oetjen, H., Ingham, T.,  
8 Stone, D., Whalley, L. K., Evans, M. J., Pilling, M. J., Leigh, R. J., Monks, P. S., Karunaharan,  
9 A., Vaughan, S., Arnold, S. R., Tschritter, J., Pöhler, D., Frieß, U., Holla, R., Mendes, L. M.,  
10 Lopez, H., Faria, B., Manning, A. J., and Wallace, D. W. R.: Seasonal characteristics of tropical  
11 marine boundary layer air measured at the Cape Verde Atmospheric Observatory, *J. Atmos.*  
12 *Chem.*, 67, 87-140, 10.1007/s10874-011-9206-1, 2011.

13 Carpenter, L. J., MacDonald, S. M., Shaw, M. D., Kumar, R., Saunders, R. W., Parthipan, R.,  
14 Wilson, J., and Plane, J. M. C.: Atmospheric iodine levels influenced by sea surface emissions of  
15 inorganic iodine, *Nature Geosci*, 6, 108-111, 10.1038/ngeo1687, 2013.

16 Carpenter, L. J., Andrews, S. J., Lidster, R. T., Saiz-Lopez, A., Fernandez-Sanchez, M., Bloss,  
17 W. J., Ouyang, B., and Jones, R. L.: A nocturnal atmospheric loss of  
18  $\text{CH}_2\text{I}_2$  in the remote marine boundary layer, *J. Atmos. Chem.*,  
19 10.1007/s10874-015-9320-6, 2015.

1 Fernandez, R. P., Salawitch, R. J., Kinnison, D. E., Lamarque, J. F., and Saiz-Lopez, A.:  
2 Bromine partitioning in the tropical tropopause layer: implications for stratospheric injection,  
3 *Atmos. Chem. Phys.*, 14, 13391-13410, 10.5194/acp-14-13391-2014, 2014.

4 Frisch, M., Trucks, G., Schlegel, H., Scuseria, G., Robb, M., Cheeseman, J., Scalmani, G.,  
5 Barone, V., Mennucci, B., and Petersson, G.: *Gaussian 09, Revision A. 1*. Wallingford, CT:  
6 Gaussian, in, Inc, 2009.

7 Georgievskii, Y., and Klippenstein, S. J.: Long-range transition state theory, *J. Chem. Phys.*, 122,  
8 194103, doi: 10.1063/1.1899603, 2005.

9 Gilbert, R. G., and Smith, S. C.: *Theory of Unimolecular and Recombination Reactions*,  
10 Blackwell, Oxford, 1990.

11 Glukhovtsev, M. N., Pross, A., McGrath, M. P., and Radom, L.: Extension of Gaussian-2 (G2)  
12 theory to bromine- and iodine-containing molecules: Use of effective core potentials, *J. Chem.*  
13 *Phys.*, 103, 1878-1885, 1995.

14 Gomez Martin, J. C., Galvez, O., Baeza-Romero, M. T., Ingham, T., Plane, J. M. C., and Blitz,  
15 M. A.: On the mechanism of iodine oxide particle formation, *Phys. Chem. Chem. Phys.*, 15,  
16 15612-15622, 10.1039/c3cp51217g, 2013.

17 Gómez Martín, J. C., Mahajan, A. S., Hay, T. D., Prados-Román, C., Ordóñez, C., MacDonald,  
18 S. M., Plane, J. M. C., Sorribas, M., Gil, M., Paredes Mora, J. F., Agama Reyes, M. V., Oram, D.  
19 E., Leedham, E., and Saiz-Lopez, A.: Iodine chemistry in the eastern Pacific marine boundary  
20 layer, *Journal of Geophysical Research: Atmospheres*, 118, 887-904, 10.1002/jgrd.50132, 2013.

- 1 Großmann, K., Frieß, U., Peters, E., Wittrock, F., Lampel, J., Yilmaz, S., Tschritter, J.,  
2 Sommariva, R., von Glasow, R., Quack, B., Krüger, K., Pfeilsticker, K., and Platt, U.: Iodine  
3 monoxide in the Western Pacific marine boundary layer, *Atmos. Chem. Phys.*, 13, 3363-3378,  
4 10.5194/acp-13-3363-2013, 2013.
- 5 Hoffmann, T., O'Dowd, C. D., and Seinfeld, J. H.: Iodine oxide homogeneous nucleation: An  
6 explanation for coastal new particle production, *Geophys. Res. Lett.*, 28, 1949-1952, 2001.
- 7 Holmes, N. S., Adams, J. W., and Crowley, J. N.: Uptake and reaction of HOI and IONO<sub>2</sub> on  
8 frozen and dry NaCl/NaBr surfaces and H<sub>2</sub>SO<sub>4</sub>, *Phys. Chem. Chem. Phys.*, 3, 1679-1687,  
9 10.1039/b100247n, 2001.
- 10 Jones, C. E., Hornsby, K. E., Sommariva, R., Dunk, R. M., von Glasow, R., McFiggans, G., and  
11 Carpenter, L. J.: Quantifying the contribution of marine organic gases to atmospheric iodine,  
12 *Geophys. Res. Lett.*, 37, L18804, 2010.
- 13 Kaltsoyannis, N., and Plane, J. M. C.: Quantum chemical calculations on a selection of iodine-  
14 containing species (IO, OIO, INO<sub>3</sub>, (IO)<sub>2</sub>, I<sub>2</sub>O<sub>3</sub>, I<sub>2</sub>O<sub>4</sub> and I<sub>2</sub>O<sub>5</sub>) of importance in the atmosphere.,  
15 *Phys. Chem. Chem. Phys.*, 10, 1723-1733, 2008.
- 16 Lamarque, J. F., Emmons, L. K., Hess, P. G., Kinnison, D. E., Tilmes, S., Vitt, F., Heald, C. L.,  
17 Holland, E. A., Lauritzen, P. H., Neu, J., Orlando, J. J., Rasch, P. J., and Tyndall, G. K.: CAM-  
18 chem: description and evaluation of interactive atmospheric chemistry in the Community Earth  
19 System Model, *Geosci. Model Dev.*, 5, 369-411, 10.5194/gmd-5-369-2012, 2012.
- 20 Lawler, M. J., Mahajan, A. S., Saiz-Lopez, A., and Saltzman, E. S.: Observations of I<sub>2</sub> at a  
21 remote marine site, *Atmos. Chem. Phys.*, 14, 2669-2678, 10.5194/acp-14-2669-2014, 2014.

1 Lee, J. D., Moller, S. J., Read, K. A., Lewis, A. C., Mendes, L., and Carpenter, L. J.: Year-round  
2 measurements of nitrogen oxides and ozone in the tropical North Atlantic marine boundary layer,  
3 *Journal of Geophysical Research: Atmospheres*, 114, n/a-n/a, 10.1029/2009jd011878, 2009.

4 Lee, J. D., McFiggans, G., Allan, J. D., Baker, A. R., Ball, S. M., Benton, A. K., Carpenter, L. J.,  
5 Commane, R., Finley, B. D., Evans, M., Fuentes, E., Furneaux, K., Goddard, A., Good, N.,  
6 Hamilton, J. F., Heard, D. E., Herrmann, H., Hollingsworth, A., Hopkins, J. R., Ingham, T.,  
7 Irwin, M., Jones, C. E., Jones, R. L., Keene, W. C., Lawler, M. J., Lehmann, S., Lewis, A. C.,  
8 Long, M. S., Mahajan, A., Methven, J., Moller, S. J., Müller, K., Müller, T., Niedermeier, N.,  
9 O'Doherty, S., Oetjen, H., Plane, J. M. C., Pszenny, A. A. P., Read, K. A., Saiz-Lopez, A.,  
10 Saltzman, E. S., Sander, R., von Glasow, R., Whalley, L., Wiedensohler, A., and Young, D.:  
11 Reactive Halogens in the Marine Boundary Layer (RHAMBLE): the tropical North Atlantic  
12 experiments, *Atmos. Chem. Phys.*, 10, 1031-1055, 10.5194/acp-10-1031-2010, 2010.

13 Leigh, R. J., Ball, S. M., Whitehead, J., Leblanc, C., Shillings, A. J. L., Mahajan, A. S., Oetjen,  
14 H., Dorsey, J. R., Gallagher, M., Jones, R. L., Plane, J. M. C., Potin, P., and McFiggans, G.:  
15 Measurements and modelling of molecular iodine emissions, transport and photodestruction in  
16 the coastal region around Roscoff, *Atmos. Chem. Phys.*, 10, 11823-11838, 2010.

17 MacDonald, S. M., Gómez Martín, J. C., Chance, R., Warriner, S., Saiz-Lopez, A., Carpenter, L.  
18 J., and Plane, J. M. C.: A laboratory characterisation of inorganic iodine emissions from the sea  
19 surface: dependence on oceanic variables and parameterisation for global modelling, *Atmos.*  
20 *Chem. Phys.*, 14, 5841-5852, 10.5194/acp-14-5841-2014, 2014.

1 Mahajan, A. S., Oetjen, H., Saiz-Lopez, A., Lee, J. D., McFiggans, G. B., and Plane, J. M. C.:  
2 Reactive iodine species in a semi-polluted environment, *Geophys. Res. Lett.*, 36, L16803,  
3 doi:16810.11029/12009GL038018, 2009.

4 Mahajan, A. S., Plane, J. M. C., Oetjen, H., Mendes, L., Saunders, R. W., Saiz-Lopez, A., Jones,  
5 C. E., Carpenter, L. J., and McFiggans, G. B.: Measurement and modelling of tropospheric  
6 reactive halogen species over the tropical Atlantic Ocean, *Atmos. Chem. Phys.*, 10, 4611-4624,  
7 2010a.

8 Mahajan, A. S., Shaw, M., Oetjen, H., Hornsby, K. E., Carpenter, L. J., Kaleschke, L., Tian-  
9 Kunze, X., Lee, J. D., Moller, S. J., Edwards, P., Commane, R., Ingham, T., Heard, D. E., and  
10 Plane, J. M. C.: Evidence of reactive iodine chemistry in the Arctic boundary layer, *J. Geophys.*  
11 *Res.*, [Atmos.], 115, D20303, doi:10.1029/2009JD013665, 2010b.

12 Mahajan, A. S., Gómez Martín, J. C., Hay, T. D., Royer, S. J., Yvon-Lewis, S., Liu, Y., Hu, L.,  
13 Prados-Roman, C., Ordóñez, C., Plane, J. M. C., and Saiz-Lopez, A.: Latitudinal distribution of  
14 reactive iodine in the Eastern Pacific and its link to open ocean sources, *Atmos. Chem. Phys.*, 12,  
15 11609-11617, 10.5194/acp-12-11609-2012, 2012.

16 McFiggans, G., Coe, H., Burgess, R., Allan, J., Cubison, M., Alfarra, M. R., Saunders, R., Saiz-  
17 Lopez, A., Plane, J. M. C., Wevill, D. J., Carpenter, L. J., Rickard, A. R., and Monks, P. S.:  
18 Direct evidence for coastal iodine particles from *Laminaria* macroalgae - linkage to emissions of  
19 molecular iodine, *Atmos. Chem. Phys.*, 4, 701-713, 2004.

1 Nakano, Y., Ukeguchi, H., and Ishiwata, T.: Rate constant of the reaction of NO<sub>3</sub> with CH<sub>2</sub>I<sub>2</sub>  
2 measured with use of cavity ring-down spectroscopy, *Chem. Phys. Lett.*, 430, 235-239, doi:  
3 10.1016/j.cplett.2006.09.002, 2006.

4 O'Dowd, C. D., Jimenez, J. L., Bahreini, R., Flagan, R. C., Seinfeld, J. H., Hameri, K., Pirjola,  
5 L., Kulmala, M., Jennings, S. G., and Hoffmann, T.: Marine aerosol formation from biogenic  
6 iodine emissions, *Nature*, 417, 632-636, 2002.

7 Ordóñez, C., Lamarque, J. F., Tilmes, S., Kinnison, D. E., Atlas, E. L., Blake, D. R., Sousa  
8 Santos, G., Brasseur, G., and Saiz-Lopez, A.: Bromine and iodine chemistry in a global  
9 chemistry-climate model: description and evaluation of very short-lived oceanic sources, *Atmos.*  
10 *Chem. Phys.*, 12, 1423-1447, 10.5194/acp-12-1423-2012, 2012.

11 Plane, J. M. C., Joseph, D. M., Allan, B. J., Ashworth, S. H., and Francisco, J. S.: An  
12 Experimental and Theoretical Study of the Reactions OIO + NO and OIO + OH, *J. Phys. Chem.*  
13 *A*, 110, 93-100, 2006.

14 Prados-Roman, C., Cuevas, C. A., Fernandez, R. P., Kinnison, D. E., Lamarque, J. F., and Saiz-  
15 Lopez, A.: A negative feedback between anthropogenic ozone pollution and enhanced ocean  
16 emissions of iodine, *Atmos. Chem. Phys.*, 15, 2215-2224, 10.5194/acp-15-2215-2015, 2015a.

17 Prados-Roman, C., Cuevas, C. A., Hay, T., Fernandez, R. P., Mahajan, A. S., Royer, S. J., Galí,  
18 M., Simó, R., Dachs, J., Großmann, K., Kinnison, D. E., Lamarque, J. F., and Saiz-Lopez, A.:  
19 Iodine oxide in the global marine boundary layer, *Atmos. Chem. Phys.*, 15, 583-593,  
20 10.5194/acp-15-583-2015, 2015b.

1 Read, K. A., Mahajan, A. S., Carpenter, L. J., Evans, M. J., Faria, B. V. E., Heard, D. E.,  
2 Hopkins, J. R., Lee, J. D., Moller, S. J., Lewis, A. C., Mendes, L., McQuaid, J. B., Oetjen, H.,  
3 Saiz-Lopez, A., Pilling, M. J., and Plane, J. M. C.: Extensive halogen-mediated ozone  
4 destruction over the tropical Atlantic Ocean, *Nature*, 453, 1232-1235, 2008.

5 Read, K. A., Lee, J. D., Lewis, A. C., Moller, S. J., Mendes, L., and Carpenter, L. J.: Intra-annual  
6 cycles of NMVOC in the tropical marine boundary layer and their use for interpreting seasonal  
7 variability in CO, *Journal of Geophysical Research: Atmospheres*, 114, n/a-n/a,  
8 10.1029/2009jd011879, 2009.

9 Roberston, S. H., Glowacki, D. R., Liang, C. H., Morley, C., Shannon, R., Blitz, M., and Pilling,  
10 M. J.: MESMER (Master Equation Solver for Multi-Energy Well Reactions), 2008–2012: An  
11 object oriented C++ program for carrying out ME calculations and eigenvalue-eigenvector  
12 analysis on arbitrary multiple well systems, edited. [Available at  
13 <http://sourceforge.net/projects/mesmer>.], in, 4.1 ed., 2014.

14 Roscoe, H. K., Jones, A. E., Brough, N., Weller, R., Saiz-Lopez, A., Mahajan, A. S.,  
15 Schoenhardt, A., Burrows, J. P., and Fleming, Z. L.: Particles and iodine compounds in coastal  
16 Antarctica, *Journal of Geophysical Research: Atmospheres*, 120, 7144-7156,  
17 10.1002/2015jd023301, 2015.

18 Saiz-Lopez, A., and Plane, J. M. C.: Novel iodine chemistry in the marine boundary layer,  
19 *Geophys. Res. Lett.*, 31, L04112, 2004.

20 Saiz-Lopez, A., Plane, J. M. C., Mahajan, A. S., Anderson, P. S., Bauguitte, S. J.-B., Jones, A.  
21 E., Roscoe, H. K., Salmon, R. A., Bloss, W. J., Lee, J. D., and Heard, D. E.: On the vertical

1 distribution of boundary layer halogens over coastal Antarctica: implications for O<sub>3</sub>, HO<sub>x</sub>, NO<sub>x</sub>  
2 and the Hg lifetime, *Atmos. Chem. Phys.*, 8, 887-900, 2008.

3 Saiz-Lopez, A., Lamarque, J.-F., Kinnison, D., Tilmes, S., Ordóñez, C., Orlando, J. J., Conley,  
4 A. J., Plane, J. M. C., Mahajan, A., Sousa Santos, G., Atlas, E., Blake, D. R., Sander, S. P.,  
5 Schaffler, S. M., Thompson, A. M., and Brasseur, G.: Estimating the climate significance of  
6 halogen-driven ozone loss in the tropical marine troposphere, *Atmos. Chem. Phys.*, 12, 3939-  
7 3949, 2012a.

8 Saiz-Lopez, A., Plane, J. M. C., Baker, A. R., Carpenter, L. J., Von Glasow, R., Gómez Martín,  
9 J. C., McFiggans, G., and Saunders, R. W.: Atmospheric Chemistry of Iodine, *Chem. Rev.*  
10 (Washington, DC, U. S.), 112, 1773-1804, 10.1021/cr200029u, 2012b.

11 Saiz-Lopez, A., Fernandez, R. P., Ordóñez, C., Kinnison, D. E., Gómez Martín, J. C., Lamarque,  
12 J. F., and Tilmes, S.: Iodine chemistry in the troposphere and its effect on ozone, *Atmos. Chem.*  
13 *Phys.*, 14, 13119-13143, 10.5194/acp-14-13119-2014, 2014.

14 Saiz-Lopez, A., Baidar, S., Cuevas, C. A., Koenig, T. K., Fernandez, R. P., Dix, B., Kinnison, D.  
15 E., Lamarque, J. F., Rodriguez-Lloveras, X., Campos, T. L., and Volkamer, R.: Injection of  
16 iodine to the stratosphere, *Geophys. Res. Lett.*, n/a-n/a, 10.1002/2015gl064796, 2015.

17 Sander, S. P., Orkin, V. L., Kurylo, M. J., Golden, D. M., Huie, R. E., Kolb, C. E., Finlayson-  
18 Pitts, B. J., Molina, M. J., Friedl, R. R., Ravishankara, A. R., Moortgat, G. K., Keller-Rudek, H.,  
19 and Wine, P. H.: Chemical kinetics and photochemical data for use in atmospheric studies, JPL-  
20 NASA, 2006.



1 Sherwen, T., Evans, M. J., Carpenter, L. J., Andrews, S. J., Lidster, R. T., Dix, B., Koenig, T. K.,  
2 Sinreich, R., Ortega, I., Volkamer, R., Saiz-Lopez, A., Prados-Roman, C., Mahajan, A. S., and  
3 Ordóñez, C.: Iodine's impact on tropospheric oxidants: a global model study in GEOS-Chem,  
4 *Atmos. Chem. Phys.*, 16, 1161-1186, 10.5194/acp-16-1161-2016, 2016.

5 Simpson, W. R., Brown, S. S., Saiz-Lopez, A., Thornton, J. A., and Glasow, R. v.: Tropospheric  
6 Halogen Chemistry: Sources, Cycling, and Impacts, *Chem. Rev.*, 115, 4035-4062,  
7 10.1021/cr5006638, 2015.

8 Sommariva, R., Bloss, W. J., and von Glasow, R.: Uncertainties in gas-phase atmospheric iodine  
9 chemistry, *Atmos. Environ.*, 57, 219-232, doi: 10.1016/j.atmosenv.2012.04.032, 2012.

10 Volkamer, R., Baidar, S., Campos, T. L., Coburn, S., DiGangi, J. P., Dix, B., Eloranta, E. W.,  
11 Koenig, T. K., Morley, B., Ortega, I., Pierce, B. R., Reeves, M., Sinreich, R., Wang, S., Zondlo,  
12 M. A., and Romashkin, P. A.: Aircraft measurements of BrO, IO, glyoxal, NO<sub>2</sub>, H<sub>2</sub>O, O<sub>2</sub>-O<sub>2</sub>  
13 and aerosol extinction profiles in the tropics: comparison with aircraft-/ship-based in situ and  
14 lidar measurements, *Atmos. Meas. Tech.*, 8, 2121-2148, 10.5194/amt-8-2121-2015, 2015.

15 von Glasow, R., Sander, R., Bott, A., and Crutzen, P. J.: Modeling halogen chemistry in the  
16 marine boundary layer. 1. Cloud-free MBL, *J. Geophys. Res.*, 107, 4341, 2002.

17 Wachsmuth, M., Gäggeler, H. W., von Glasow, R., and Ammann, M.: Accommodation  
18 coefficient of HOBr on deliquescent sodium bromide aerosol particles, *Atmos. Chem. Phys.*, 2,  
19 121-131, 10.5194/acp-2-121-2002, 2002.

20 Wang, F., Saiz-Lopez, A., Mahajan, A. S., Gómez Martín, J. C., Armstrong, D., Lemes, M., Hay,  
21 T., and Prados-Roman, C.: Enhanced production of oxidised mercury over the tropical Pacific

1 Ocean: a key missing oxidation pathway, *Atmos. Chem. Phys.*, 14, 1323-1335, 10.5194/acp-14-

2 1323-2014, 2014.

3

4

1 **Tables**

2

3 Table 1: Night time reactions of emitted inorganic iodine compounds considered in addition to  
 4 the iodine chemistry scheme used by (Saiz-Lopez et al., 2014).

No.	Reaction	Notes
R1.	$I_2 + NO_3 \rightarrow I + IONO_2$	$1.5 \times 10^{-12} \text{ cm}^3 \text{ molecule}^{-1} \text{ s}^{-1}$ [ <i>Chambers et al.</i> , 1992]
R2.	$HOI + NO_2 \rightarrow I + HNO_3$	Endothermic by $9 \text{ kJ mol}^{-1}$ and the transition state is $73 \text{ kJ mol}^{-1}$ above the reactants
R3.	$HOI + HNO_3 \rightarrow IONO_2 + H_2O$	Exothermic by $11 \text{ kJ mol}^{-1}$ . The reaction first forms a complex $21 \text{ kJ mol}^{-1}$ below the reactants but this rearranges to the products via a transition state that is $110 \text{ kJ mol}^{-1}$ above the reactants.
R4.	$HOI + NO_3 \rightarrow IO + HNO_3$	Exothermic by $11 \text{ kJ mol}^{-1}$ with all transition states below the reactants.  $k(T) = 2.7 \times 10^{-12} (300 \text{ K} / T)^{2.66} \text{ cm}^3 \text{ molecule}^{-1} \text{ s}^{-1}$

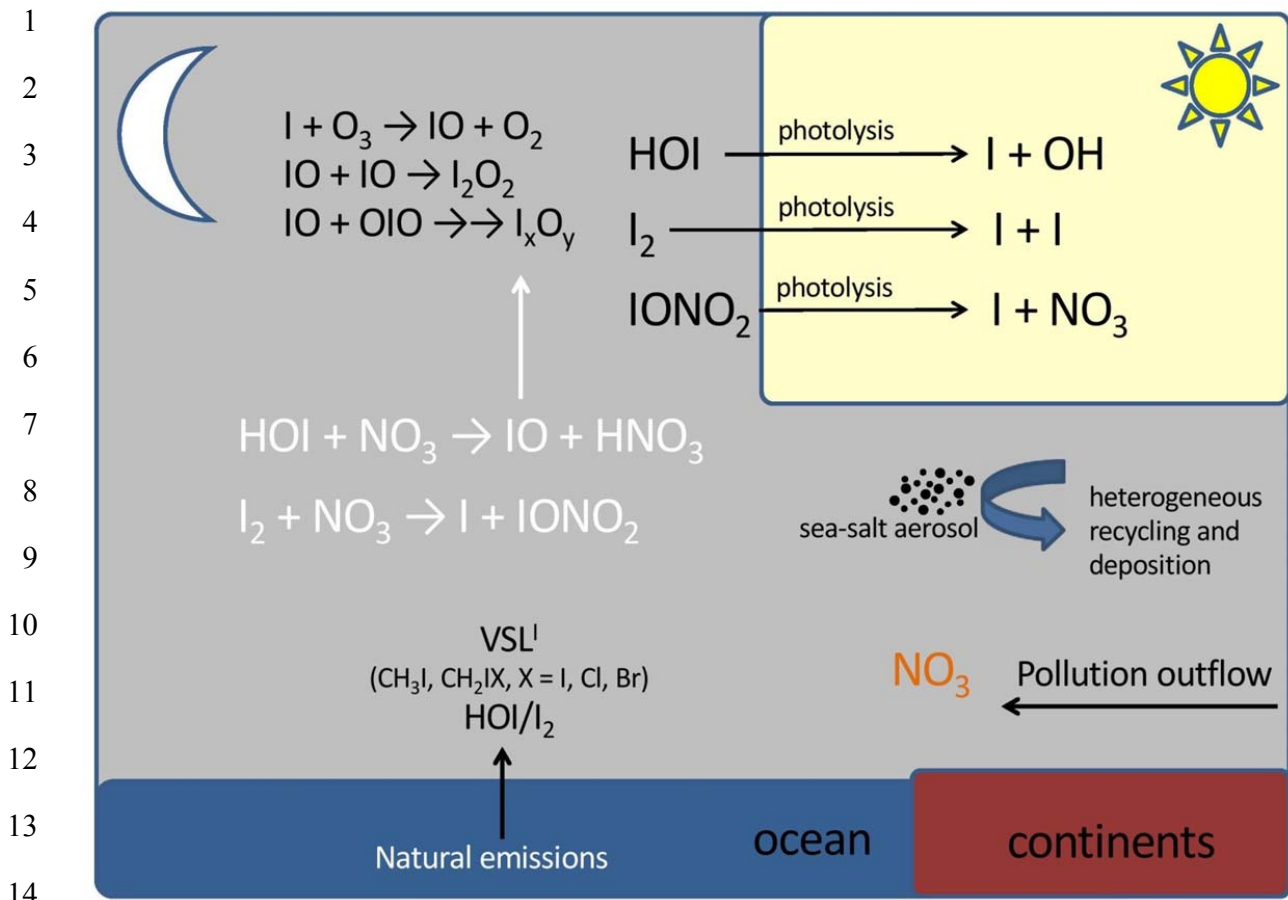
5

6

1 **Table 2.** Calculated vibrational frequencies, rotational constants and energies of the stationary  
 2 points and asymptotes on the HOI + NO<sub>3</sub> doublet potential energy surface

Species	Geometry <sup>a</sup>	Vibrational frequencies <sup>b</sup>	Rotational constants <sup>c</sup>	Potential energy <sup>d</sup>
HOI + NO <sub>3</sub>		603, 1084, 3803 & 261, 261, 805, 1108, 1108, 1126	623.9, 8.182, 8.076 & 13.84, 13.84, 6.919	0.0
IOH-NO <sub>3</sub> complex	O 1.623, 0.284, -0.331 H 1.484, -0.657, -0.043 I 0.009, 1.205, 0.286 N -0.456, -2.265, 0.030 O -1.052, -3.321, -0.0473 O -1.147, -1.195, -0.228 O 0.742, -2.161, 0.333	55, 84, 118, 161, 196, 615, 629, 667, 705, 803, 968, 1228, 1273, 1491, 3268	5.610, 0.916, 0.806	-24.0
IO-H-NO <sub>2</sub> TS	O 0.309, 1.515, 0.247 H -0.834, 1.314, -0.017 I 1.280, -0.089, -0.093 N -2.349, -0.133, 0.019 O -3.518, -0.429, -0.035 O -1.444, -0.962, 0.257 O -2.019, 1.117, -0.187	1249i, 70, 97, 103, 225, 472, 676, 698, 797, 806, 1041, 1147, 1308, 1513, 1626	6.300, 0.864, 0.767	-16.4
IO-HNO <sub>3</sub> complex	O 0.571, 1.350, 0.348 H -1.111, 1.098, -0.020 I 1.870, 0.0645, -0.152 N -2.503, -0.202, 0.0186 O -3.673, -0.396, -0.170 O -1.654, -0.986, 0.401 O -2.081, 1.090, -0.242	35, 43, 76, 126, 198, 623, 677, 703, 772, 798, 939, 1331, 1416, 1713, 3281	7.058, 0.605, 0.566	-34.8
IO + HNO <sub>3</sub>		648 & 477, 585, 649, 782, 901, 1320, 1345, 1738, 3724	9.844 & 13.01, 12.05, 6.258	-10.6

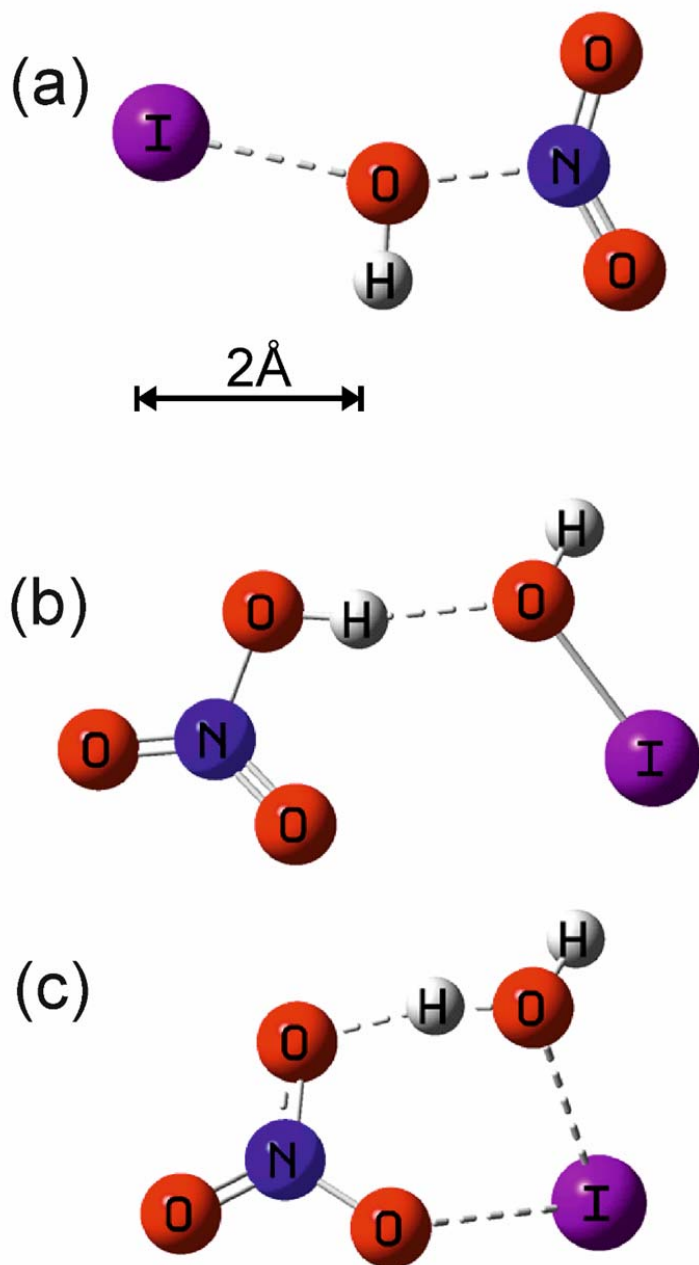
3 <sup>a</sup> Cartesian co-ordinates in Å. <sup>b</sup> In cm<sup>-1</sup>. <sup>c</sup> In GHz. <sup>d</sup> In kJ mol<sup>-1</sup>, including zero-point energy and spin-  
 4 orbit coupling of I and IO (see text).



15 **Figure 1.** New nocturnal iodine chemistry (in white) implemented in the THAMO and CAM-  
16 Chem models.

17  
18  
19  
20  
21  
22  
23  
24  
25

1



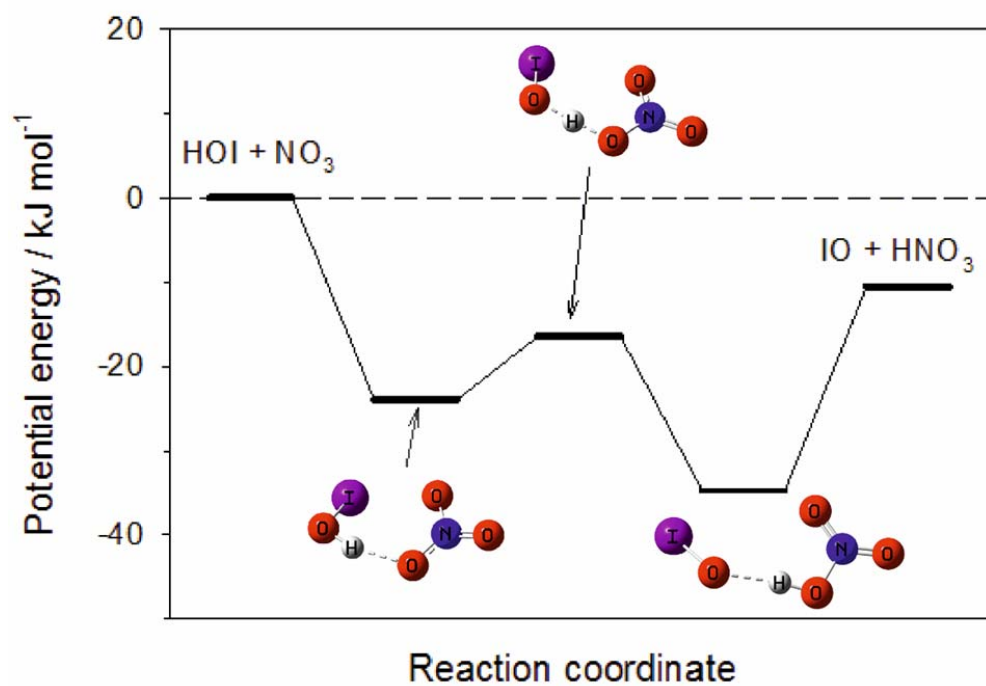
2

3

4

5 **Figure 2:** (a) Transition state for the reaction between HOI and NO<sub>2</sub> to form HNO<sub>3</sub> + I; (b)  
6 complex formed between HOI and HNO<sub>3</sub>, which then reacts via transition state (c) to form  
7 IONO<sub>2</sub> + H<sub>2</sub>O.

1

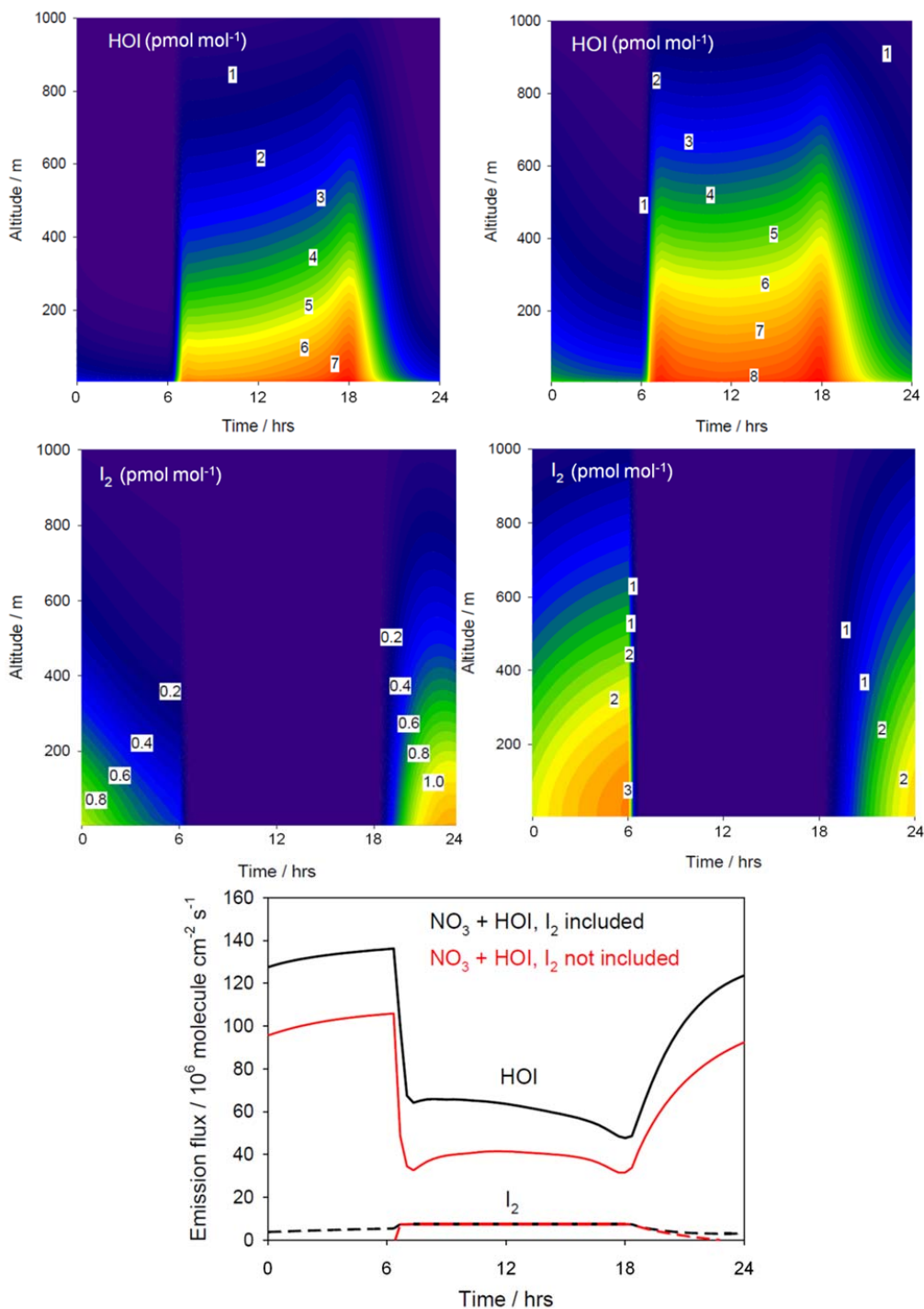


2

3

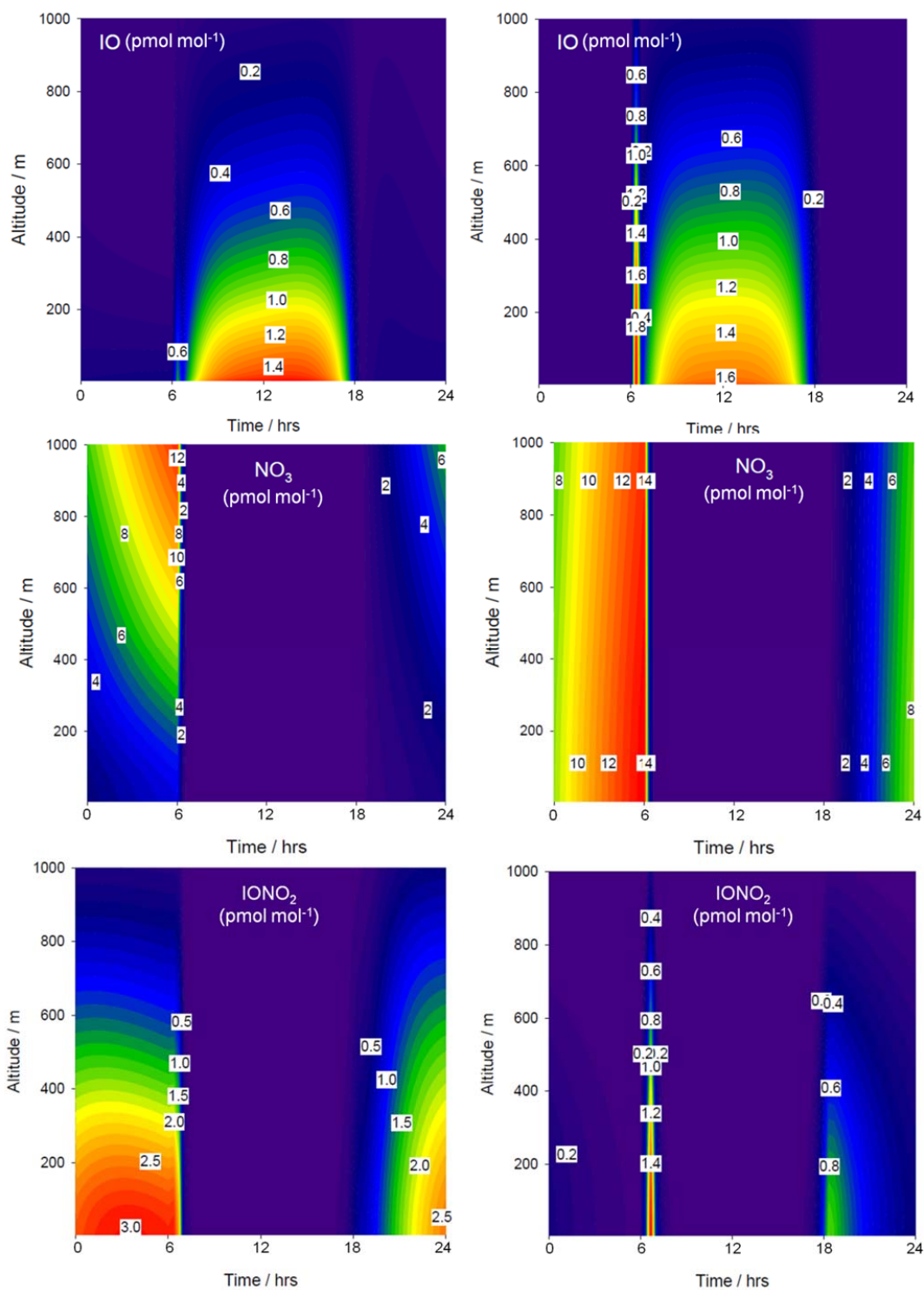
4 **Figure 3.** Potential energy surface for the reaction between HOI and NO<sub>3</sub>, which contains two  
5 intermediate complexes separated by a submerged barrier.

6

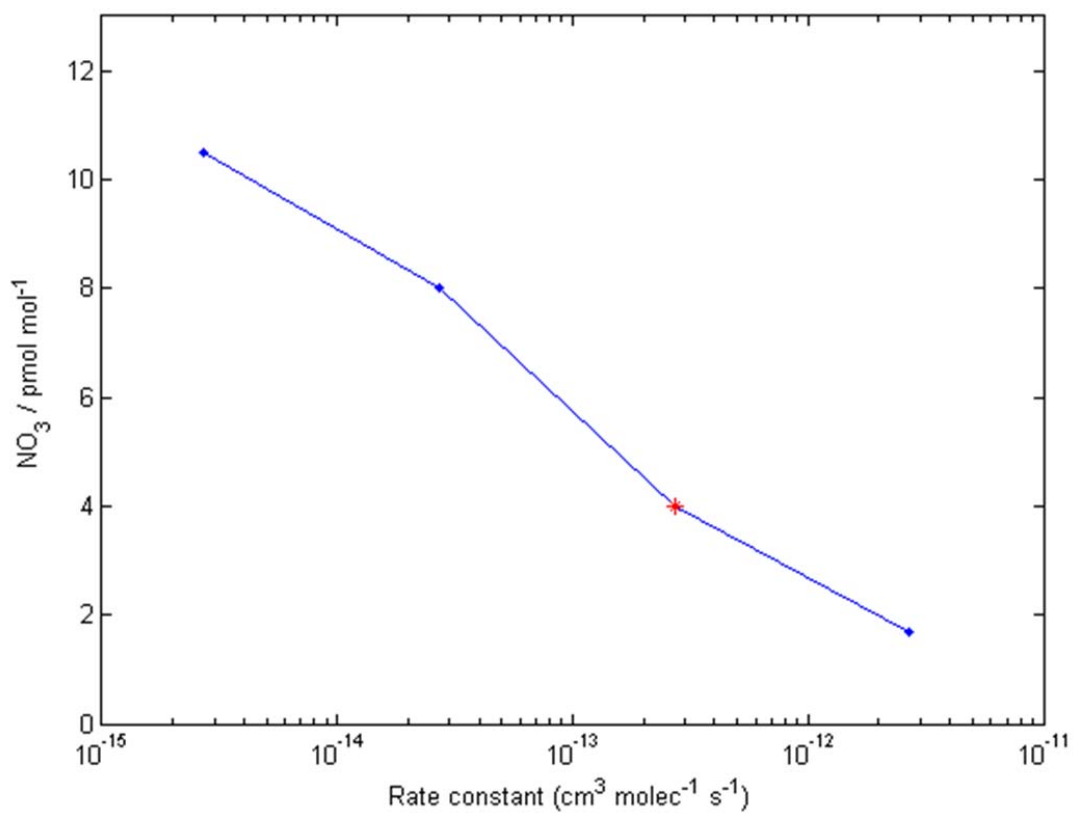


1  
 2 **Figure 4.** THAMO modeled diurnal variation of HOI, I<sub>2</sub> (upper panels) and the HOI/I<sub>2</sub> flux from  
 3 the ocean surface (bottom panel). The right hand panels are from scenario 1, which do not  
 4 include night time reactions of HOI and I<sub>2</sub> with NO<sub>3</sub>, while the left hand panels include the  
 5 reactions in scenario 2. In bottom panel red lines represent scenario 1, while black lines  
 6 correspond to scenario 2.



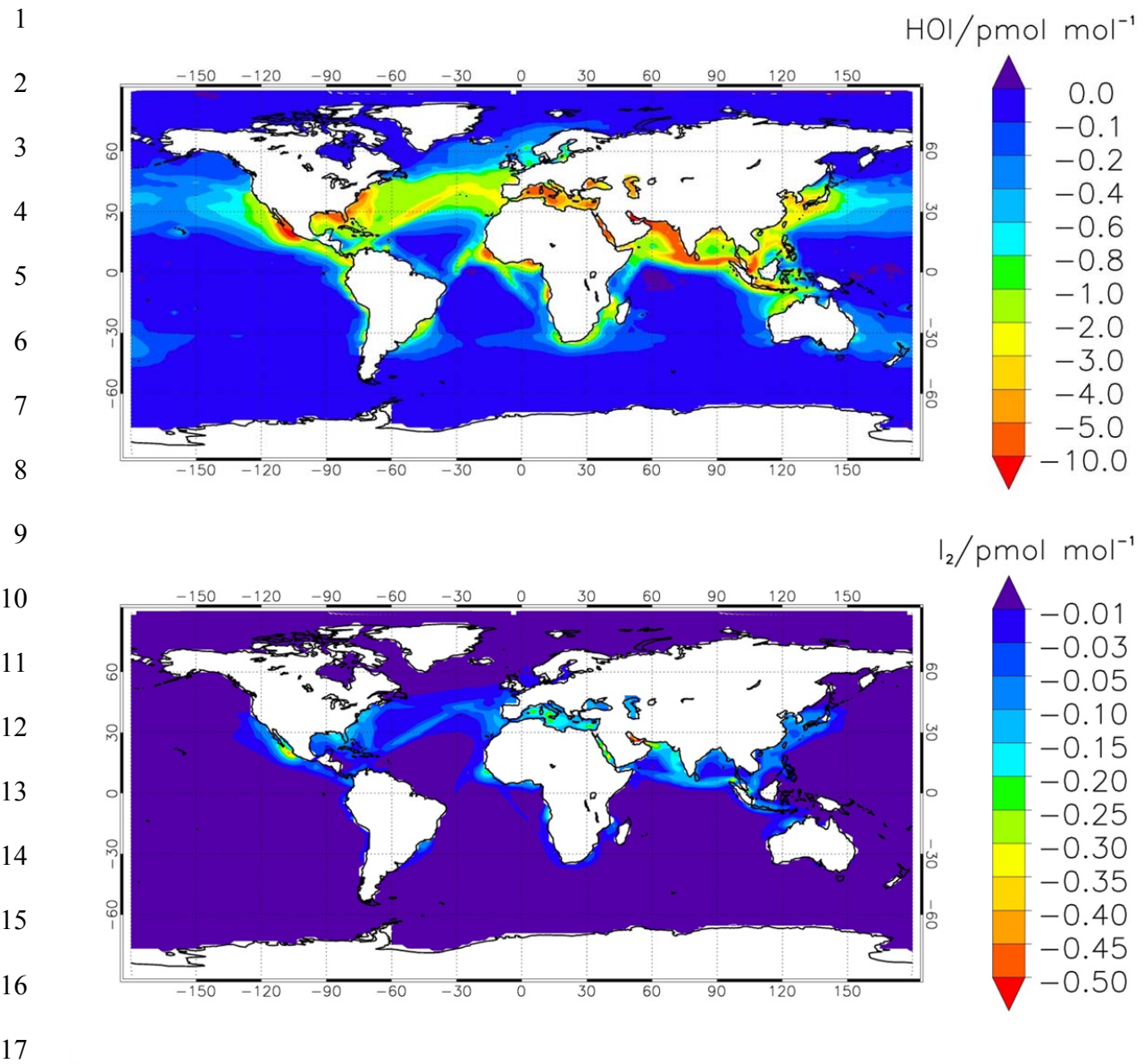


1  
 2 **Figure 5.** THAMO modeled diurnal variation of IO, NO<sub>3</sub> and the IONO<sub>2</sub>. The right hand panels  
 3 are from scenario 1, which do not include night time reactions of HOI and I<sub>2</sub> with NO<sub>3</sub>, while the  
 4 left hand panels include the reactions in scenario 2.



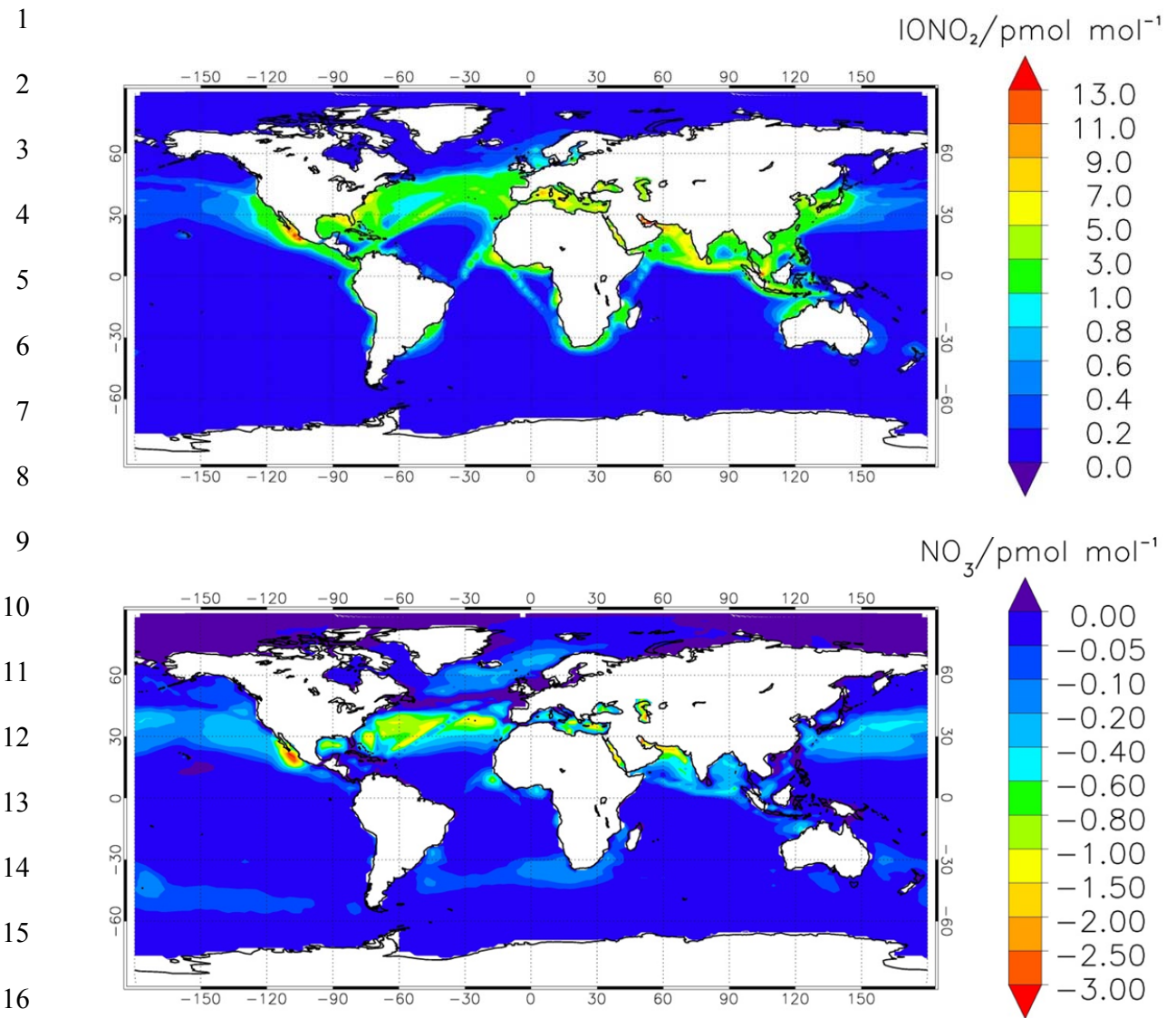
1  
2 **Figure 6.** Sensitivity run showing the effect of the uncertainty in the rate constant estimation on  
3 the reduction of NO<sub>3</sub> at the surface - the red point is the theoretical estimate.

4  
5  
6  
7  
8  
9  
10  
11



18 **Figure 7.** Modelled annual average of HOI (a) and  $\text{I}_2$  (b) during night time at the surface level.  
 19 The panels show the difference in volume mixing ratio between the simulations with and without  
 20 reactions (1) and (4).

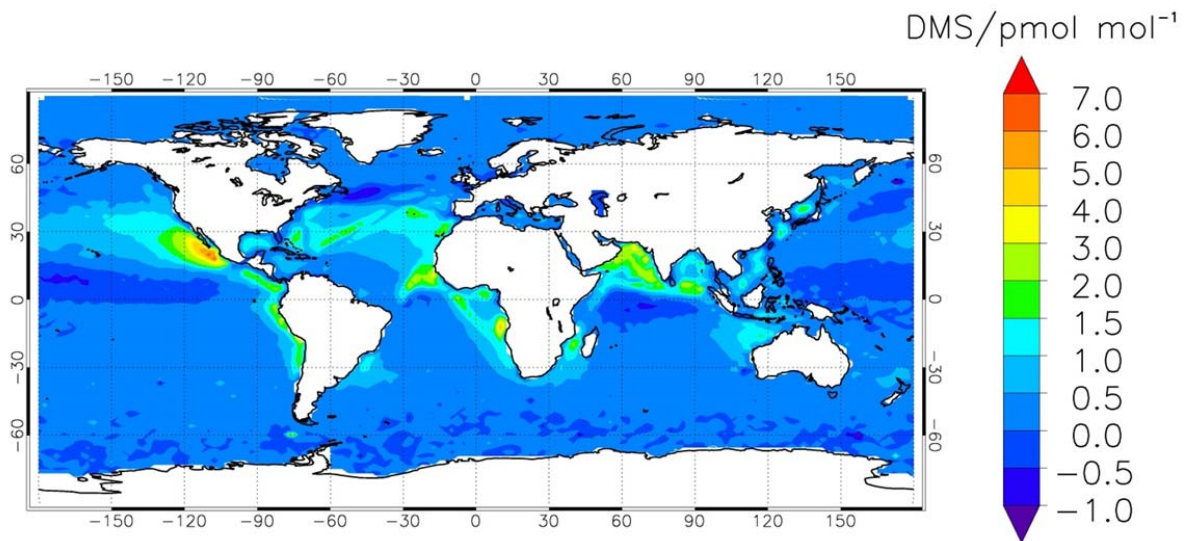
21



18 **Figure 8.** Modelled annual average of  $\text{IONO}_2$  (a) and  $\text{NO}_3$  (b) during night time at the surface  
 19 level, as the difference in volume mixing ratio between the simulations with and without  
 20 reactions (1) and (4).

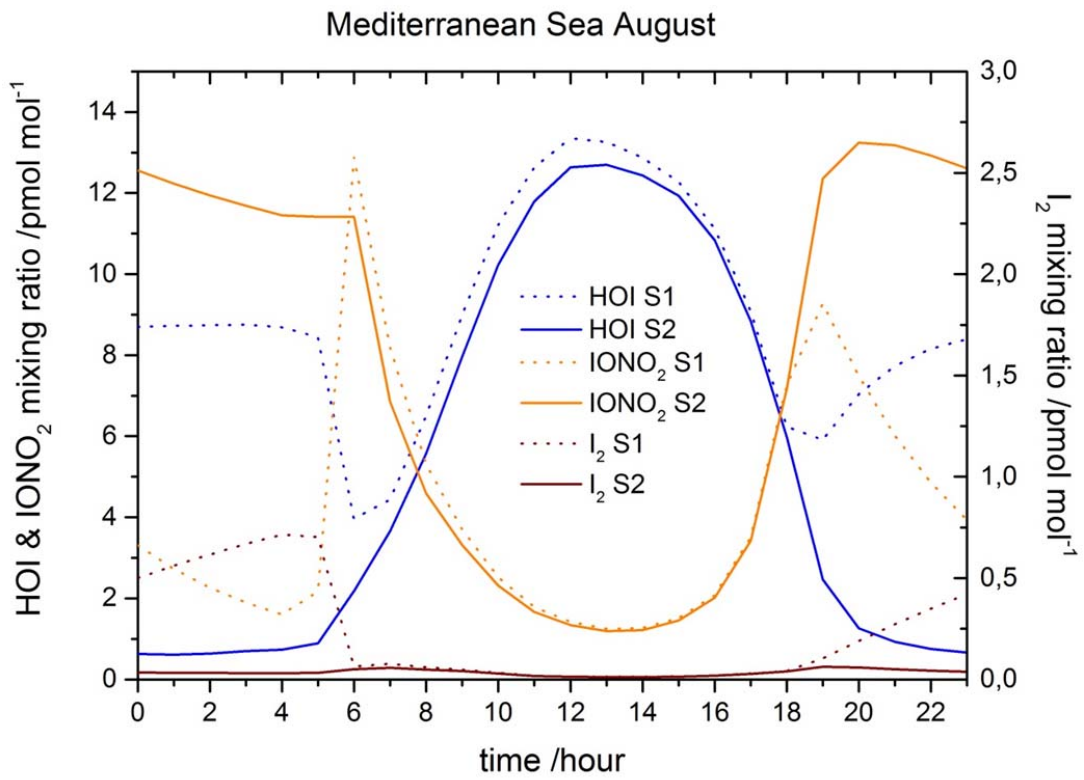
21

1  
2  
3  
4  
5  
6  
7  
8  
9  
10  
11  
12  
13  
14  
15  
16  
17  
18  
19  
20  
21  
22  
23  
24



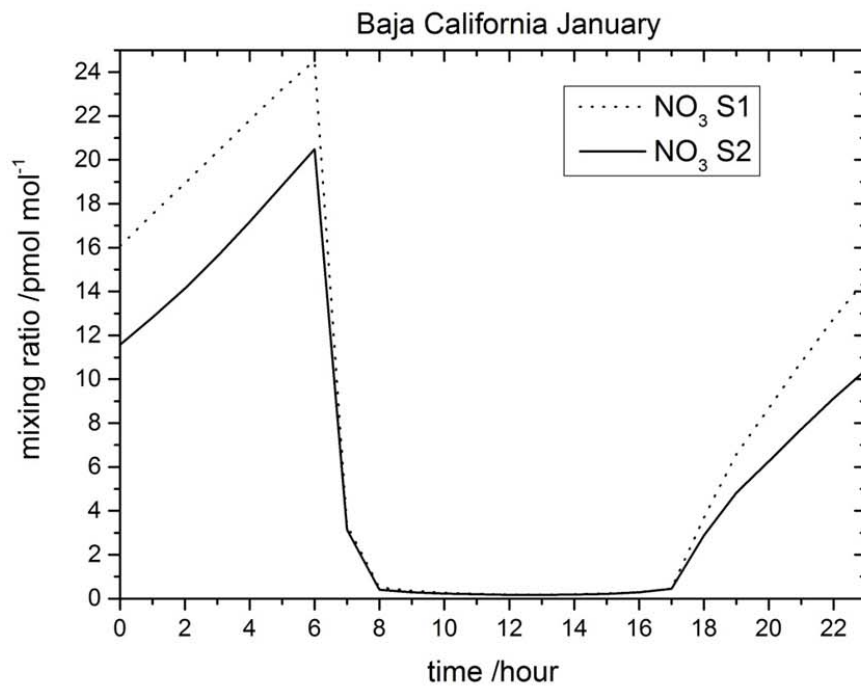
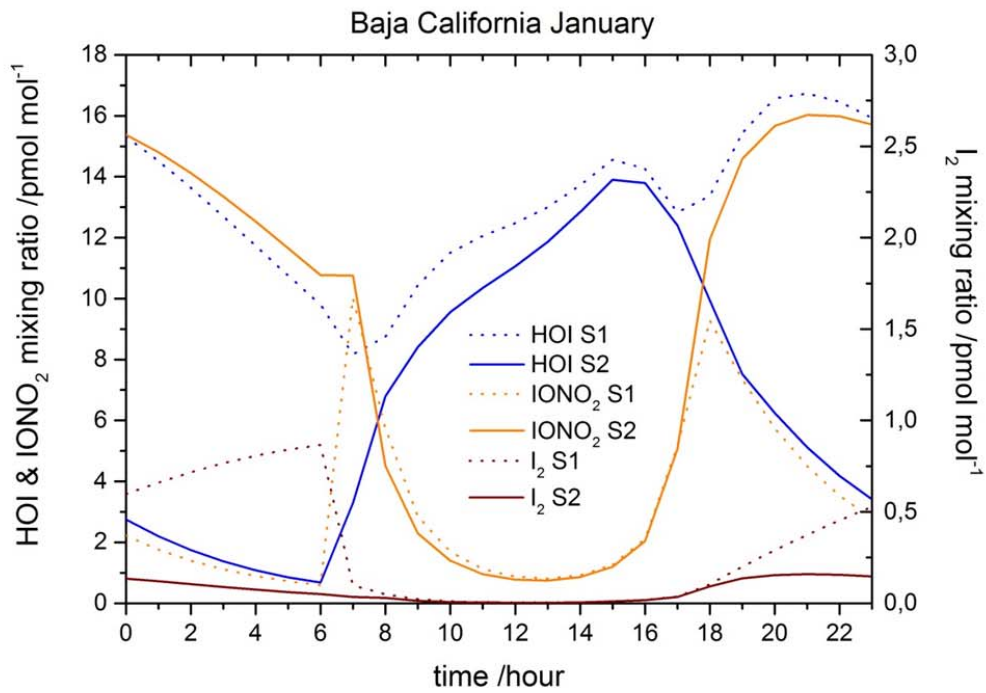
**Figure 9.** Increase in the DMS levels during night time at the surface level due to the inclusion of the reactions R1 and R4 in CAM-Chem.

1  
2  
3  
4  
5  
6  
7  
8  
9  
10  
11  
12  
13  
14  
15  
16  
17  
18  
19  
20  
21  
22  
23  
24



**Figure 10.** Hourly averaged concentration of HOI, IONO<sub>2</sub> and I<sub>2</sub> in the Mediterranean Sea at the surface level (lon:10°→20°E, lat:33°→40°N)





22 **Figure 11.** Hourly averaged concentration of HOI, IONO<sub>2</sub> and I<sub>2</sub> (upper panel) and NO<sub>3</sub> (bottom  
 23 panel) in the Pacific Ocean at the south of Baja California peninsula at the surface level  
 24 (lon: -110°→-106°E, lat:16°→23°N)